922

440

Copy

TECHNICAL MEMORANDUMS

NATIONAL ADVISORY COMMITTEE FOR AERONAUTICS

No. 970

EXPERIMENTAL INVESTIGATIONS ON FREELY EXPOSED DUCTED RADIATORS

By W. Linke

Jahrbuch 1938
der Deutschen Luftfahrtforschung

Washington
March 1941

NATIONAL ADVISORY COMMITTEE FOR AERONAUTICS

TECHNICAL MEMORANDUM NO. 970

EXPERIMENTAL INVESTIGATIONS ON FREELY EXPOSED DUCTED RADIATORS*

By W. Linke

SUMMARY

The present report deals with the relation between the open areas, the drag, and the air flow as observed on freely exposed, ducted radiators - the air conductivity being modified from zero to one unit. The most advantageous forms of ducts are derived therefrom.

In conjunction with theoretical results, the individual components of the drag of ducted radiators are discussed and general rules established for low-loss ducts. The influence of the wall thickness of the ducts, of the length ratio of the exit, and the effects of sonic velocity on diffusers are dealt with by special measurements.

INTRODUCTION

The enclosure of radiator elements on an airplane usually consists in placing these elements in a duct with entrance and exit area smaller than the frontal area of the block. On such radiators, fitted with diffuser and exit - termed, for short, "ducted radiator" - a reduction in the drag per unit of heat dissipation, is secured in comparison to the blocks freely exposed to the air stream or, in other words, a reduction in the ratio

$$\frac{\text{Cooling drag } W}{\text{Heat transfer } Q}$$

is achieved. The usual explanation is as follows: The drag W consists largely of flow resistance, approximately proportional to the square of the flow velocity v.

---

*"Experimentelle Untersuchungen an freifahrenden Düsenkühlern." Jahrbuch 1938 der Deutschen Luftfahrtforschung, pp. II 281-292.

The heat transfer Q, however, varies approximately as the first power of the velocity. Therefore, the ratio W/Q decreases with v and it appears advantageous to cool at lowest possible flow velocities; this is accomplished by the diffuser and exit which permit throttling of the flow as desired by reducing the percentage of open area.

But the throttling of the flow is limited for several reasons: As the heat removal abates with the flow, the frontal area - required for removing a certain amount of heat - becomes continuously greater and with it also the weight and volume of the system by reduction in flow. Furthermore, by this procedure, the area necessary for ducting increases; i.e., additional drag occurs which, together with the increased weight, might nullify the achieved gains, altogether.

It is of interest to know the amount by which the ratio of entrance or exit area to frontal area of radiator, can be safely reduced and how the diffuser and the exit can be designed so as to keep the additional drag to a minimum. The present report is intended as a contribution to the experimental clarification of these aspects. The effect of the open areas on the drag and air flow was measured on an installed cooling system and explored with screens throughout the entire range of air conductivity. This afforded first, data concerning suitable opening ratios with their entailed drag and cooling performances; second, a general review over the combined action of the air conductivity of installed systems, air flow, opening ratios and drag, which includes not only radiator elements but also air-cooled engines with very little conductivity.

With the use of unheated screens, the effect of air heating on the drag and the flow was at first disregarded. A separate study, wherein these effects are explored on an electrically heated radiator block, will not be discussed here. Merely results, so far as necessary, for consideration of air heating on the screen measurements, are recounted.

Lastly, it is pointed out, all experiments were conducted at low air speeds; hence, effects which at high flying speeds entail the approach of sonic velocity at different parts of radiator ducts, were disregarded. The restrictions imposed hereby are discussed separately.

II. TEST PROCEDURE

The measurements were conducted on freely exposed ducted radiators, and for the following reasons: First, because this simpler case was to be treated; second, because measurements on complete airplane bodies by the dimensions of the Aachen wind tunnel (jet diameter, 1.85 m) had led to very small frontal areas, and hence to a not-very-accurate determination of the effect of the opening ratios. Lastly, with the choice of freely exposed radiator, the frontal area of the radiator could be made so large that original radiator blocks of 200 by 300 mm^2 frontal area, previously explored for heat removal and pressure drop in a closed channel, could be installed in the ducts. The radiator frontal area itself, 200 by 300 mm^2, was rectangular. The ducts with different open areas were obtained by different assemblies of one base duct subdivisible at sections a (fig. 1). By these means, the entrance areas could be varied from 0 percent (duct closed), 13 percent, 36 percent, 66 percent, to 100 percent; and the exit areas from 0 percent, 15 percent, 34 percent, 65 percent, to 100 percent of the radiator frontal area. The entrance areas are hereinafter denoted by V_0, V_{13}, V_{36}, etc., and the exit areas by H_0, H_{15}, H_{34}, etc. The duct had a double wall (plywood inside and outside), thus affording a smooth wall despite the combination and rounding off of the corners of the rectangular section. Breakaway of flow and turbulence were to be avoided by a fairly great length and the use of nose and tail fairings (b in fig. 1). These measures entailed, of course, a fairly heavy wall thickness of the duct, the effects of which are discussed later on.

The use of screens afforded a ready means of ascertaining the range of variation of the conductivity from 0 to 1. By conductivity is meant the value:

$$\eta_{ai} = \frac{1}{\sqrt{1 + \frac{\Delta p}{\frac{\rho v^2}{2}}}} \qquad (1)$$

where v rate of flow

Δp pressure drop on screen or radiator block at speed v

The use of this conductivity concept is advantageous to the extent that η_{ai} can be dealt with as constant for any system provided the rate of flow is not too low, which would not be the case to the same extent if - say, the drag coefficient $c_w = \frac{\Delta p}{\frac{\rho}{2} v^2}$ were used for the aerodynamic characterization of a conductive body. The conductivity η_{ai} may assume values between 0 and 1. And, in the case that the pressure of undisturbed flow is reached directly behind the freely exposed radiator, while entailing no energy losses before and behind the radiator due to breakdown of flow or friction, it also has the significance of the ratio of flow velocity v to flying speed v_o; hence, $\eta_{ai} = v/v_o$ (reference 1).

Four different screens, shown with conductivity plotted against rate of flow in figure 2, were used. For higher rates of flow, where the square resistance law applies to the separate elements (wires) of the screens, the values $\eta_{ai} = 0.183$; 0.358; 0.466; 0.270 were assumed. These figures are applied throughout to identify the screens, even when the particular rate of flow was small and η_{ai}, strictly speaking, was smaller. Other than the four conductivities, there are the conductivities $\eta_{ai} = 0$ (board inserted) and $\eta_{ai} = 1$ (free passage). The normal conductivity of radiators ranges between 0.3 and 0.5; in radial engines, between 0.05 and 0.15.

Lastly, a cold radiator block, 180 mm deep, was inserted, the conductivity of which is also given in figure 2. It closely agrees with that of the screen $\eta_{ai} = 0.466$, and so afforded a check on the equality of radiator and screen in regard to resistance and flow.

The drag and flow measurements were conducted at all possible combinations of opening ratio and conductivity. The resistance was recorded by balance as usual, at $v_o = 15$, 30, and 40 m/s air speed. The mean flow velocity v was obtained by graphical integration of 35 separate measurements scattered over the section of the screen with the Prandtl pitot tube (fig. 1) at $v_o = 30$ m/s air speed.

For observation of the previously cited effect of radiator heating, a modern water radiator (tubes with

streamlined section and indirect cooling surfaces) was set in the duct and heated electrically, each tube containing a heating coil.

III. RESULTS OF TESTS AND DISCUSSION

a) Flow and Resistance

Table I contains the recorded mean flow velocities v (nondimensional) in relation to $\eta_{ai} = v/v_o$; further, the recorded drag W as drag coefficient

$$c_{w_o} = \frac{W}{F \frac{\rho}{2} v_o^2}$$

(F = radiator frontal area = 0.0615 m^2; to differentiate from the maximum section area F' = 0.0983 m^2). Figures 3 and 4 show η_{ae} and c_{w_o} plotted against η_{ai}. According to figure 3, $\eta_{ae} = \eta_{ai}$ at $V_{100}H_{100}$; i.e., for this duct, merely representing a frame around the radiator, the previously cited simple conditions prevail. The c_{w_o} values manifest a certain systematic aspect, at which the formation of a maximum at average η_{ai} values and not too small opening ratios, is noteworthy and which is interrupted only by V_{100} and especially by small η_{ai} through abrupt resistance increases. Observations with streamers proved this to be due to the breakdown of the flow on the front edge of the duct. In regard to this phenomenon, figure 5, which gives the c_{w_o} values for several ducts at different speeds v_o, discloses its appearance, especially at small Reynolds numbers. Apart from the breakdown phenomena, only minor scale effects are noticeable, hence the c_{w_o} values for v_o = 40 m/s, substantially retain their validity even at large Reynolds numbers.

Anticipating, according to the foregoing, adherence of flow at larger Reynolds numbers than employed in the test and with a view of clarifying the connections between drag, flow, and conductivity, the drag coefficients recorded by breakdown of flow were extrapolated to those for adhering flow by means of the graphs of figure 6. In this representation c_{w_o} is plotted for constant η_{ai} over a system of coordinates, giving in one direction the opening

ratios of the air entrance and at right angles to the air exit. Instead of the irregular, high-drag coefficients at breakdown of flow, the systems in this representation can be easily brought into conformity with adhering flow. Figure 6 further contains the c_{w_o}' values referred to maximum cross-sectional area F' of fuselage, not to frontal area F of the radiator. It is now readily seen by how much the drag of a ducted radiator is greater than the streamline body V_oH_o, to which every form can be restored. The coefficient of the body V_oH_o amounts to $c_{w_o}' = 0.066$. The extrapolated values are shown dotted and bracketed in figure 4.

A radiator block of the same conductivity as the screen $\eta_{ai} = 0.466$ was, as already stated, built in the duct. It consisted of air tubes of rectangular 3 x 8.5 mm^2 section, and 180 mm depth. In table II the c_{w_o} and η_{ae} values of screen and radiator are compared for several ducts. They show, on the whole, good agreement between radiator and screen, except for ducts at V_{100} where the radiator drag is a little lower. This might be due to a directional effect of the radiator tubes, although the tests do not exactly substantiate this conclusion.

In furtherance of the discussion, we show c_{w_o} plotted against η_{ae} in figure 7 for all the observed arrangements by constant η_{ai}. The test points are connected by lines of constant entrance and exit area, and so afford a graph in which c_{w_o} and η_{ae} can be interpolated for any not-recorded opening ratios. The opening ratios, for which the drag becomes minimum for certain flow η_{ae}, are located on the lower boundary curve of the graphs. Ducts for which c_{w_o}/η_{ae} reaches a minimum, correspond to the contact points of the tangents drawn from the zero point to the lower boundary curve. Whereas on this lower curve the exit areas pass through all values, the entrance areas are contingent upon the condition that they are greater at small η_{ae} than the exit areas and greater than the conductivity η_{ai} of the built-in screen by higher η_{ae} values, but otherwise of any magnitude. In other words, the conditions*

---

*See footnote, p. 7

$$V > H$$

and

$$V \geq \eta_{ai}$$

hold true. Regarding these conditions, the following should be borne in mind: In exposing a diffuser to free flow, the flow will always break down on the inner wall of the diffuser - as indicated in figure 8 - if certain diffuser angles are exceeded. To make the flow adhere in the diffuser, which would require a pressure rise in it

$$p_1 - p_o = \frac{\rho}{2} v_1^2 \left(\left(\frac{F_1}{F_o} \right)^2 - 1 \right) \qquad (2)$$

(fig. 8), an exit or a conductive body is fitted behind the diffuser, with at least the same pressure rise $p_1 - p_o$ before it, and hence the same flow deceleration in free flow. This is the case for exits with opening ratio equal to or smaller than that of the diffuser and by adherence of outside flow to the exit. It holds true for conductive bodies with conductivity η_{ai} equal to or smaller than the ratio F_o/F_1 of the diffuser, and when the pressure p_o of undisturbed flow is reached behind the body as, say, on the duct $V_{100}\ H_{100}$. The Δp of such bodies follows (cf. equation (1)):

$$\Delta p = \frac{\rho}{2} v^2 \left(\frac{1}{\eta_{ai}^2} - 1 \right) \qquad (3)$$

The conditions $V > H$ and $V > \eta_{ai}$ for the lower boundary curve therefore imply that on it the flow in the diffuser adheres, whereas at all other points above it, breakdown of flow has taken place.

This point is of special significance for the control of ducted radiators. Theoretically, the control must always be such as to satisfy the foregoing conditions, in order to avoid needless resistance and flow decreases

---

*(From p. 6)

Several test points for $V_{100}H_{100}$ at small η_{ae}, which are not located on the lower boundary curve, do not satisfy those conditions. However, since uncertain extrapolated test points are involved (breakdown outside), this behavior is disregarded here.

through breakdown in the diffuser. To illustrate: Using for a radiator with $\eta_{ai} = 0.4$, the opening ratios $V_{60}H_{23}$ as high-speed setting, the raising of the flow is preferably accomplished by opening the exit areas, and to any desired percentage without fear of breakdown of flow in the diffuser, because V is always greater than η_{ai}. But with $V_{30}H_{23}$ as setting for high speed, the entrance area would also have to be enlarged at least to V_{40} if on opening of the exit areas, H_{30} is reached. So, if the control is to be confined to the exit area and the location on the lower boundary curve is to be retained, the entrance area must not be less than the conductivity.

From the drag of the eddy-free ducts on the lower boundary curve, one minimum drag can be segregated that would exist, when the observed flow η_{ae}, is due only to momentum losses in the cooling block itself, and otherwise no other drag of any kind occurs. This minimum drag is computed according to formulas originally employed by R. S. Capon (reference 2) from the recorded flow η_{ae}, when the conductivity η_{ai} is introduced and assumed to be known. If there are no losses upstream or downstream from the cooling block, and the pressures and speeds are such as indicated in figure 9, the momentum equation defines the minimum drag W*, when placing a control surface at great distance around the ducted radiator, so that the pressure integral becomes equal to zero:

$$W^* = F \rho v_1 (v_o - v_2) \tag{4}$$

In the region upstream and downstream from the radiator block, Bernoulli's equation can be applied, i.e.:

$$\left.\begin{aligned} p_o + \frac{\rho}{2} v_o^2 &= p_1 + \frac{\rho}{2} v_1^2 \\ p_o + \frac{\rho}{2} v_2^2 &= p_2 + \frac{\rho}{2} v_1^2 \end{aligned}\right\} \tag{5}$$

Equations (4) and (5) together with

$$\eta_{ae} = \frac{v_1}{v_o}, \qquad \eta_{ai} = \frac{1}{\sqrt{1 + \dfrac{\Delta p}{\frac{\rho}{2} v_1^2}}}$$

give as coefficient $c_{w_o}{}^* = \frac{W^*}{\frac{\rho}{2} v_o^2 F}$ of the minimum drag:

$$c_{w_o}{}^* = 2\eta_{ae}\left(1 - \sqrt{1 - \eta_{ae}{}^2\left(\frac{1}{\eta_{ae}{}^2} - 1\right)}\right) \qquad (6)$$

This minimum W^* can be divided into a cooling-block drag $(= W_K = (p_1 - p_2) F)$ and a duct drag W_V. The corresponding coefficients are $c_{w_o K}$ and $c_{w_o V}$.

With

$$\Delta p = \left(\frac{1}{\eta_{ai}{}^2} - 1\right) \frac{\rho}{2} v_1{}^2$$

it affords for

$$c_{w_o K} = \Delta p \, F \, \frac{\rho}{2} v_o{}^2 F$$

$$c_{w_o K} = \left(\frac{1}{\eta_{ai}{}^2} - 1\right) \eta_{ae}{}^2 \qquad (7)$$

The duct drag coefficient $c_{w_o V} = c_{w_o}{}^* - c_{w_o K}$ is, as will be shown, always negative; i.e., suction forces appear on the duct.

For the specific case, $\eta_{ae} = \eta_{ai}$, which for duct $V_{100} H_{100}$ occurs usually, on other ducts only at small η_{ai} (fig. 3) (Townend rings included), equations (6) and (7) reduce to

$$c_{w_o}{}^* = 2\eta_{ai}\,(1 - \eta_{ai}) \qquad (6a)$$

and

$$c_{w_o K} = 1 - \eta_{ai}{}^2 \qquad (7a)$$

hence the consistently negative value

$$c_{w_o V} = -\,(1 - \eta_{ai})^2 \qquad (8)$$

for the duct drag coefficient.

The coefficients c_{w_o}* and c_{w_oK}, plotted in figure 7, disclose the consistently negative duct drag very plainly. In no case do the test points of the lower boundary curve reach the minimum drag coefficients. The difference between the two curves represents largely the cumulative drag due to friction on the inside and outside wall of the duct. It is, upon closer examination - at $\eta_{ai} = 1$, directly apparent - fairly constant for different ducts, flows, and conductivities. In the graphical representation of figure 10, the different drag proportions are outlined in detail.

The propulsive forces created on the ducts were directly recorded on designs $V_{100}H_{100}$ and $V_{66}H_{100}$ and the pressure distributions integrated. To this end, pressure orifices were fitted on V_{66} H_{100} at two sections of the diffuser, conformable to figure 11, and on a section of the rear edge (b in fig. 1), on $V_{100}H_{100}$ at only one section each of the front and the rear edge of the duct. Figures 12 and 13 give the results for various η_{ai} values. As expected, the outside of the diffusers manifest severe low pressures which, on the $V_{100}H_{100}$ rise to four times the dynamic pressure q_o by decreasing η_{ai}, and on the $V_{66}H_{100}$ to 2.6 times. The multiples (φ) are shown separately in table III for the important practical conductivities ($\eta_{ai} = 0$ and 0.183 correspond to radial engines; $\eta_{ai} = 0.358$ and 0.466 to cooling systems). The flying speeds $\overline{v}_o$ at which, according to Bernoulli, the sonic velocity corresponding to the momentary φ value is reached on the diffuser, represent speed limits at which the present data are best applicable. They manifest the extent to which sonic velocity can occur at the present flying speeds and how, by further speed increases, it is necessary to change from diffuser forms producing considerable flow deflection, and hence high increase of speeds, to slender (small diameter) forms.

The coefficients c_{w_oV} obtained from the pressure distributions by planimetry are shown in figures 14 and 15, subtracted from the related c_{w_oK} values. This difference $c_{w_oK} - c_{w_oV}$, which represents the total drag when the frictional drag is discounted is, on the whole, in close agreement with the minimum drag coefficients

c_{w_o}* (broken curve). The theoretically expected propulsion $c_{w_oK} - c_{w_o}$* is therefore fully developed on the duct. That this happens by $V_{100}H_{100}$ also, where at small η_{ai} outside breakdown of flow takes place, can be explained by the fact that here only pressure distributions were recorded on one section - i.e., the wide side of the duct, where the low pressures are higher than on the narrow side, and then used to define c_{w_oV}. The propulsive forces are therefore a little too great. The high position of the point for $V_{66}H_{100}$ and $\eta_{ai} = 0.720$ is attributable to breakdown of flow inside of the diffuser ($V < \eta_{ai}$), as manifested on the pressure distribution curve.

b) Additional Measurements on Thin-Walled Radiators in Ducts

Between the minimum drag c_{w_o}* and the eddy-free drag c_{w_o} of the lower boundary curve, there existed a fairly high, approximately constant difference, which is chiefly due to friction drag. This is, in part, attributable to the comparatively great wall thickness of the ducts and it appeared desirable to ascertain the extent to which this drag reduces if the walls are thinner. For this purpose, several other ducts of ratio $\frac{F}{F'} = 0.90$ as against the previous $\frac{F}{F'} = 0.62$ were explored (fig. 16). The entrance area was assumed constant at 66 percent of the frontal surface, the exit areas at 0, 12, 66, 85, and 100 percent (identification $V_{66}H_{12}d$). The radiator walls, being considerably thinner than those studied previously (fig. 16), could be measured in the small wind tunnel of the Institute (v_o = 40 m/s). The frontal surface was circular. The conductivities of the screens amounted to $\eta_{ai} = 0.205$, 0.32, 0.435, and 0.685. This time the flow was obtained by recording the pressure drop at two orifices of the cylindrical centerpiece of the ducts. The test data are appended in table IV, while in figure 17, the c_{w_o} and c_{w_o}* values are shown plotted against η_{ae}. Since, on the whole, $V > \eta_{ai}$ and $V > H$, the c_{w_o} curves correspond to the lower boundary curves in figure 7. It is seen that the additional drag is approximately

equal to the previously obtained values only when $\eta_{ae} = 0$, that is, H_o; it reaches considerably lower values with increasing exit area. Still lower c_{w_o} curves should be difficult to obtain. For the rest, the findings - aside from the smaller differences $c_{w_o} - c_{w_o}{}^*$ - are in close agreement with the previous data. The different constant, the different shape of frontal surface, and the use of a different wind tunnel, speak for the general validity of the other measurements.

Other than this wall-thickness effect, the change of the additional drag exceeding the minimum drag by changes in the exit length l, was also deemed of enough importance to study it on three ducts with equal open areas $V_{66}H_{26}d$, but different ratio of exit length l to radiator frontal area diameter D $\left(\frac{l}{D} = 2.03, 1.08, \text{ and } 0.70, \text{ fig. } 16\right)$. The results are tabulated in table V, the c_{w_o} and $c_{w_o}{}^*$ values plotted against η_{ai} in figure 18. The longest exit gives the least difference in $c_{w_o} - c_{w_o}{}^*$ (fig. 18). The differences, however, are so small that, under certain conditions the shorter exits are preferable for reasons of space and weight.

In figure 19 is shown, in conclusion, the behavior of characteristic installation forms, with particular reference to minimum drag. Plotted against the conductivity are shown:

A. The drag coefficients of completely bare screens, according to Flachsbart's tests (reference 3). In addition, the minimum drag coefficient $c_{w_o}{}^{**}$, which affords a Flachsbart theory for this particular case with conductivity η_{ai}. It gives

$$c_{w_o}{}^{**} = \frac{1}{\left(\frac{1}{\eta_{ai}{}^2} - 1\right)\left(\frac{1}{4} + \frac{1}{\left(\frac{1}{\eta_{ai}{}^2} - 1\right)}\right)^2} \quad \text{for } \eta_{ai} > 0.445.$$

The agreement with the theoretical values for $\eta_{ai} \geq 0.7$ states that in this η_{ai} range, no additional drag occurs, which in this instance could consist only of separation

drag. On exceeding this range, the flow takes on the character of plate flow ($\eta_{ai} = 0$) with extended vortex zone.

B. The drag coefficients of screens in a thin-walled tube. The entrance area is not rounded off, so that at small η_{ai} values the flow surely breaks down on the outside. It relates in this instance to hitherto unmentioned tests on a duct consisting of a rectangular sheet-metal frame with 200 x 300 mm^2 frontal surface, which has the same length as $V_{100}H_{100}$ (400 mm), and the value $F/F' = 0.97$. The rate of flow was not recorded.

C. The c_{w_o} and $c_{w_o}{}^*$ values of a thin-walled duct with round outside exit area ($V_{66}H_{100}d$). The outside breakdown at small η_{ai} as in case B, has shifted to the inside of the diffuser at great η_{ai} ($V < \eta_{ai}$).

D. The c_{w_o} and $c_{w_o}{}^*$ values of a duct on which, through correct opening ratios of diffuser and exit, the breakdown of flow over the entire η_{ai} range has been eliminated - in return for which the friction drag $c_{w_o} - c_{w_o}{}^*$ of the duct is, of course, so much higher.

c) The Best Open Areas

These cannot be summarily determined from the quotients c_{w_o}/η_{ae} say, of figure 7, as indication of quality, since the cooling power is not exactly proportional to η_{ae}. Besides, it would make no allowance for the weight increase by decreasing opening ratio. The different forms are therefore evaluated on the basis that the ratio of dragging power L to cooling power $Q_e - L$ is the power required to sustain and propel the installation in level flight. In this manner, the proportion of weight and drag is expressed by one digit.

The dragging power L is approximately

$$L = v_o W + v_o \epsilon G$$

$$= \left(c_{w_o} + \frac{\epsilon g}{\frac{\rho}{2} v_o^2} \right) v_o F \frac{\rho}{2} v_o^2 = \lambda F \frac{\rho}{2} v_o^3 \qquad (9)$$

where W drag

G radiator weight

g radiator weight per unit of frontal surface

ϵ gliding angle of airplane

The cooling power Q_e itself was not recorded; it can, however, be conjugated to the different η_{ai} and η_{ae} by means of heat-dissipation measurements on cooling elements, as follows:

The cooling power Q of radiator elements is usually measured jointly with the conductivity η_{ai} in the closed tube (reference 4), figure 20. It is

$$Q = F\ v\ \gamma_L\ c_{p_L}(t_a - t_e)$$

Hence the cooling power Q_i of a radiator in free flow in the specific case of $\frac{v}{v_o} = \eta_{ai}$, existing, for instance, at $V_{100}H_{100}$:

$$Q_i = \eta_{ai} \cdot \eta_{th}\ F\ v_o\ \gamma_L\ c_{p_L}\ \theta \qquad (10)$$

where $\theta = \vartheta_m - t_e$, ϑ_m = mean coolant temperature, $\eta_{th} = \left(\frac{t_a - t_e}{\theta}\right)$. Instead of Q_i, it is expedient to consider only the nondimensional product, termed the "cooling power factor," $\eta_{ai} \cdot \eta_{th}$, shown in figure 21, plotted against η_{ai} at $v_o = 50$ m/s for different cooling systems (numbered 3, 5, 6, 8, Lo 6, and 7). The broken curve passes through those points of the individual curves in which the radiator depth $l = 300$ mm, is reached. It indicates maximum values reached at present with such depths for $v_o = 50$ m/s by different conductivities and which are not likely ever to be much higher in the future. That $\eta_{ai}\ \eta_{th} = f\ (\eta_{ai})$ has a maximum is apparent, for η_{th}; i.e., the ratio of air heating in the radiator to the temperature range in the radiator $(\vartheta_m - t_e)$ must drop monotonically from 1 at $\eta_{ai} = 0$ (extreme case, in which infinitely great cooling area is built in) to 0 at $\eta_{ai} = 1$.

Besides, since η_{ai} can never be greater than 1, the product of $\eta_{ai} \cdot \eta_{th}$ must always remain below the 45° line.

Strictly speaking, the values in figure 21 hold for $v_o = 50$ m/s only. But from the small speed effect indicated at $v_o = 30$ and 90 m/s in figure 22, its use in the following denotes no marked limitation, in general. The slight speed effect is to be expected, for - since ordinarily $Q \sim v^{0.8}$ - it follows that $\eta_{ai} \cdot \eta_{th} \sim \frac{1}{v_o^{0.2}}$ for constant η_{ai}, according to equation (10).

From these Q_i values for the extreme case $\frac{v}{v_o} = \eta_{ai}$, the values Q_e of a duct with $\frac{v}{v_o} = \eta_{ae}$ can be derived as follows: By given v_o

$$Q_i = C\, v_i^{0.8}$$

and

$$Q_e = C\, v_e^{0.8}$$

where C is the same constant, and v_i and v_e denote rate of flow in the extreme, and in the general case, respectively. Then,

$$Q_e = \left(\frac{v_e}{v_i}\right)^{0.8} Q_i = \left(\frac{\eta_{ae}}{\eta_{ai}}\right)^{0.8} \cdot \eta_{ai} \cdot \eta_{th}\, \gamma_L\, c_{p_L}\, v_o\, F \cdot \theta$$

$$= \kappa\, \gamma_L\, c_{p_L}\, v_o\, F\, \theta \qquad (11)$$

and for the desired evaluation quantity, L/Q_e

$$\frac{L}{Q_e} = \frac{\lambda}{\kappa} \frac{\frac{\rho}{2} v_o^2}{\gamma_L\, s_{p_L} \theta} \qquad (12)$$

It is sufficient to analyze the nondimensional ratio

$$\frac{\lambda}{\kappa} = \frac{c_{w_o} + \frac{\epsilon\, S}{\frac{\rho}{2} v_o^2}}{\left(\frac{\eta_{ae}}{\eta_{ai}}\right)^{0.8} \eta_{ai}\, \eta_{th}}$$

which, admittedly, is not independent of v_o, and to compute with constant values of ϵ and g. Throughout the following we put $\epsilon = 0.1$ and $g = 1.5$ kg/dm^2, so that λ can be plotted against κ, as shown in figure 23 for $\eta_{ai} = 0.358$. Owing to the relationship existing between λ and v_o, each speed v_o really should be plotted separately. But this can be avoided by plotting the summands c_{w_o} of λ upward, from a certain point of the ordinate, and the speed-related summands $\epsilon g \frac{\rho}{2} v_o^2$ downward. The opening ratios for best dragging power at different speeds are obtained by the contact points of tangents of the corresponding zero points to the ordinates. The completed process gives the best opening ratios in relation to conductivity η_{ai}, as indicated in figures 24a and 24b, along with the related η_{ae} and c_{w_o} values, and the obtained ratios λ/κ. The opening ratios and η_{ae} values, by the degree of accuracy with which they were computed, are applicable to thin-walled and thick-walled ducts. The shown c_{w_o} and λ/κ values for thin-walled ducts are those for vanishing weight effect ($v_o = \infty$). With observance of the remaining results, the representation gives the following practical points of view for the best fit of freely exposed radiators:

1) The entrance areas (fig. 24a) may range anywhere between $V = 100$ percent and $V = \eta_{ai}$,* so long as the increases in speed outside of the diffuser remain small compared with sonic velocity; i.e., at medium flying speed. At higher flying speeds, the lower permissible limits must be approached and slender diffuser form chosen. To illustrate: For speeds up to 375 m/hr, an entrance area of around 60 percent and a diffuser similar to V_{66} is recommended. (See table III.)

2) On the best ducts the exit area (fig. 24b) is usually smaller than the conductivity.

3) The weight factor disregarded (fig. 24c), a general rule for the flow is: $\eta_{ae} = \frac{1}{2} \eta_{ai}$.

---

*Herewith the demand for simple control - i.e., that of air exit - is satisfied.

4) The drag coefficient c_{w_o} (fig. 24d) is largely independent of η_{ai}. The lowest value obtainable is $c_{w_o} = 0.14$.

5) The ratio λ/κ (fig. 24e) becomes minimum at $\eta_{ai} = 0.3$ to 0.4, i.e., when the cooling-power factor of the cooling system becomes maximum.

IV. DRAGGING POWER BY BEST OPENING RATIO WITH ALLOWANCE FOR THE EFFECT OF AIR HEATING

The following is a comparison with other radiator installation designs mounted on an airplane fuselage on the basis of the obtained results, in an attempt to ascertain what part of the engine power for the cooling is stressed while using the best radiators in free stream. The weight is disregarded but not the effect of air heating, which consists in a decrease of drag and flow. The test data employed for this purpose are $\Delta W = W(\theta) - W(0)$ and $\Delta Q = Q(\theta) - Q(0)$ of table VI, which were obtained by installing a 200 mm deep, electrically heated radiator SKF RR 240 in different ducts and which, for the time being, are applicable only to these or similar systems and to low flying speeds. The values ΔW and ΔQ are those for temperature differences $\theta = 65^{\circ}$ C (water cooling). The table further contains the ratios $\psi = \frac{W(\theta)}{Q(\theta)} \frac{Q(0)}{W(0)}$, with which the values λ/κ obtained so far for weight omission, must be multiplied in order to allow for the air heating effect.

The desired dragging power is, according to equation (12):

$$L = \frac{\lambda}{\kappa} \psi \frac{\frac{\rho}{2} v_o^2 Q_e}{\gamma_L c_{p_L} \theta}$$

The Q_e is expressed by the heat dissipation required for the cooling of 1 horsepower of engine power which, for water cooling, amounts to around 320 kcal/h, and for glycol cooling, to around 250 kcal/h. Then the division of L

by the propeller efficiency (assumed at $\eta = 0.7$) gives the dragging power in portions of the engine power.

The conductivity of the radiator block is to be $\eta_{ai} = 0.35$, which corresponds to the ψ values in table VI, and to the best conductivity, according to figure 24. The respective λ/κ value is equal to 1. The entrance area is assumed as V_{66}, the exit area at H_{23}, according to figure 24. For these data the values $\psi = 0.91$ at $\theta = 65^\circ$ C, and $\psi = 0.83$ at $\theta = 114^\circ$ C, are interpolated from table VI, which finally afford:

$$L = 5.03\ 10^{-6}\ v_o^2 \text{ (hp) for } \theta = 65^\circ \text{ C}$$

$$L = 1.43\ 10^{-6}\ v_o^2 \text{ (hp) for } \theta = 114^\circ \text{ C}$$

(v_o in m/s), plotted in figure 25 in percentage of engine horsepower.

Translation by J. Vanier,
National Advisory Committee
for Aeronautics.

REFERENCES

1. Linke, W.: Windkanalmessungen an Kühlerverkleidungen Abh. a. d. Aerodyn. Inst. Aachen, Heft 15 (1938); or Jahrbuch 1937 der deutschen Luftfahrtforschung II, S. 165.

2. Capon, R. S.: The Cowling of Cooling Systems. R. & M. No. 1702, British A.R.C., 1936.

3. Flachsbart, O.: Widerstand von Seidengazefiltern, Runddraht- und Blechstreifensieben mit quadratischen Maschen. Ergebnisse d. Aerodyn. Vers.-Anstalt, Göttingen, IV, 1933.

4. Lorenz, H.: Warmeabgabe und Widerstand von Kühlerelementen. Abh. a. d. Aerodyn. Inst. Aachen, Heft 13, 1933.

Table I

Measured values c_{w_e} and η_{ae}

Duct		$\eta_{ai} = 0$		0,183		0,358		0,466		0,720		1,0	
		c_{we}	η_{ae}	c_{we}	η_{ae}	c_{we}	η_{ae}	c_{we}	η_{ae}	c_{we}	η_{ae}	c_{we}	η_{ae}
V 0	H 0	0,105	0										
	H 15	0,112	0										
	H 34	0,125	0										
	H 65	0,138	0										
	H 100	0,182	0										
V 13	H 0	0,124	0										
	H 15	0,128	0	0,165	0,072	0,166	0,063	0,166	0,077	0,167	0,088	0,169	0,184
	H 34	0,146	0	0,207	0,087	0,214	0,069	0,212	0,096	0,213	0,106	0,214	0,210
	H 65	0,160	0	0,238	0,089	0,250	0,083	0,253	0,099	0,251	0,110	0,253	0,227
	H 100	0,214	0	0,288	0,091	0,295	0,103	0,303	0,103	0,305	0,118	0,316	0,223
V 36	H 0	0,125	0										
	H 15	0,139	0	0,174	0,106	0,155	0,128	0,146	0,128	0,139	0,157	0,133	0,180
	H 34	0,151	0	0,248	0,141	0,248	0,198	0,234	0,224	0,219	0,276	0,209	0,328
	H 65	0,169	0	0,305	0,148	0,356	0,242	0,368	0,272	0,369	0,340	0,360	0,433
	H 100	0,214	0	0,373	0,158	0,469	0,285	0,506	0,319	0,500	0,375	0,409	0,494
V 66	H 0	0,134	0										
	H 15	0,144	0	0,179	0,108	0,156	0,133	0,147	0,135	0,137	0,156	0,133	0,150
	H 34	0,158	0	0,255	0,141	0,245	0,217	0,216	0,262	0,162	0,320	0,138	0,373
	H 65	0,171	0	0,315	0,159	0,373	0,285	0,370	0,369	0,289	0,521	0,184	0,620
	H 100	0,227	0	0,394	0,166	0,516	0,334	0,537	0,458	0,532	0,678	0,328	0,880
V 100	H 0	0,408[1]	0										
	H 15	0,428[1]	0	0,473[1]	0,112	0,424[1]	0,125	0,404[1]	0,139	0,388[1]	0,150	0,209[1]	0,170
	H 34	0,550[1]	0	0,526[1]	0,146	0,253	0,224	0,222	0,268	0,170	0,316	0,139	0,362
	H 65	0,582[1]	0	0,578[1]	0,156	0,382	0,294	0,374	0,366	0,277	0,528	0,142	0,619
	H 100	0,630[1]	0	0,651[1]	0,175	0,538	0,333	0,590	0,469	0,515	0,725	0,136	1,03
V 100[2]	H 0	0,136											
	H 15	0,144		0,190		0,176		0,178		0,144		0,158	
	H 34	0,163		0,260									
	H 65	0,168		0,334									
	H 100	0.240		0,420									

[1]) External flow separated
[2]) Extrapolate values for no separated flow

TABLE II

Comparison of Radiator HW Sp.R. 180 with Screen $\eta_{ai} = 0.466$

Duct	c_{w_o} radiator	c_{w_o} screen	η_{ai} radiator	η_{ae} screen
V_{36} H_{34}	0.235	0.234	0.22	0.22
V_{66} H_{65}	.372	.370	.39	.37
V_{100} H_{34}	.216	.222	.26	.27
V_{100} H_{65}	.364	.374	.38	.37
V_{100} H_{100}	.555	.590	.47	.47

TABLE III

φ and $\overline{v}_o$ Values for $V_{100}H_{100}$ and $V_{66}H_{100}$

Cowl \ η_{ai}		0	0.183	0.358	0.466
V_{100} H_{100}	φ	4.05	3.44	2.63	2.26
	$\overline{v}_o$ (km/h)	533	570	628	664
V_{66} H_{100}	φ	2.63	1.71	1.24	1.0
	$\overline{v}_o$ (km/h)	630	729	802	848

TABLE IV. Test Values of c_{w_o} and η_{ae} for Thin-Walled Ducted Radiator

	η_{ae}=0		0.205		0.32		0.435		0.685		1	
Cowl	c_{w_o}	η_{ae}	c_{w_o}	η_{ae}	c_{w_o}	η_{ae}	c_{w_o}	η_{ae}	c_{w_o}	η_{ae}	c_{w_o}	η_{ae}
$V_{66}H_{12}$	0.1142	0	0.1235	0.1015	0.113	0.1065	0.1062	0.109	0.1017	0.1685	0.0993	
$V_{66}H_{26}$	.1215	0	.1841	.1605	.1617	.190	.1369	.2085	.105	.242	.0897	
$V_{66}H_{44}$	.1322	0	.2584	.1868	.2538	.2535	.2208	.3078	.1476	.391	.0885	
$V_{66}H_{65}$	.1592	0	.2896	.1928	.3154	.2925	.3044	.355	.2184	.489	.1278	
$V_{66}H_{85}$	.1592	0	.3342	.210	.3811	.298	.3823	.396	.3342	.556	.2426	
$V_{66}H_{100}$	.205	0	.415	.206	.486	.304	.544	.426	.518	.6	.413	

TABLE V. Experimental c_{w_o} and η_{ae} for Thin-Walled Ducted Radiator $V_{66}H_{26}$ with Different Exit Length Ratio l/D

	η_{ai}=0		0.205		0.320		0.435		0.685		1	
l/D	c_{w_o}	η_{ae}	c_{w_o}	η_{ae}	c_{w_o}	η_{ae}	c_{w_o}	η_{ae}	c_{w_o}	η_{ae}	c_{w_o}	η_{ae}
0.70	0.1301	0	0.1929	0.151	0.1696	0.203	0.1545	0.197	0.1301	0.2373	0.1162	
1.08	.1134	0	.1829	.154	.1547	.205	.1441	.1995	.1227	.236	.1039	
2.03	.1215	0	.1841	.1605	.1617	.19	.1369	.2085	.105	.242	.0897	

TABLE VI

Drag and Cooling Power Reduction Due to Air Heating in the System SKF RR 240, 200

Cowl	$\theta=65^{\circ}C$			$\theta=114^{\circ}C$		
	$\frac{\Delta W}{W(0)}$	$\frac{\Delta Q}{Q(0)}$	Ψ	$\frac{\Delta W}{W(0)}$	$\frac{\Delta Q}{Q(0)}$	Ψ
V_{36} H_{65}	-0.11	-0.04	0.93	-0.19	-0.07	0.87
V_{36} H_{100}	-.08	-.07	.99	-.14	-.12	.98
V_{66} H_{15}	-.15	-.05	.89	-.26	-.09	.81
V_{66} H_{34}	-.13	-.07	.94	-.23	-.11	.85
V_{66} H_{65}	-.12	-.07	.95	-.21	-.12	.90
V_{66} H_{100}	-.09	-.06	.97	-.16	-.10	.93
$V_{100}H_{100}$	-.08	-.04	.96	-.14	-.07	.93

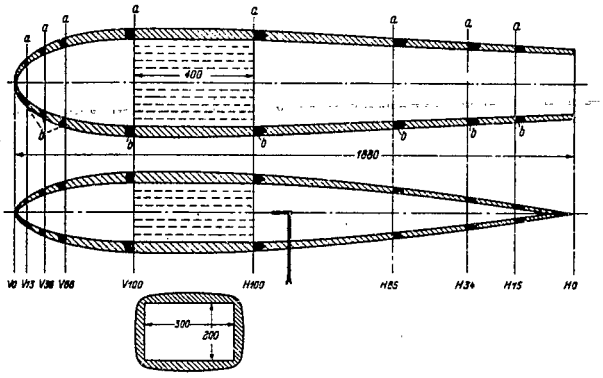

Figure 1.- Experimental ducted radiator with different open areas.

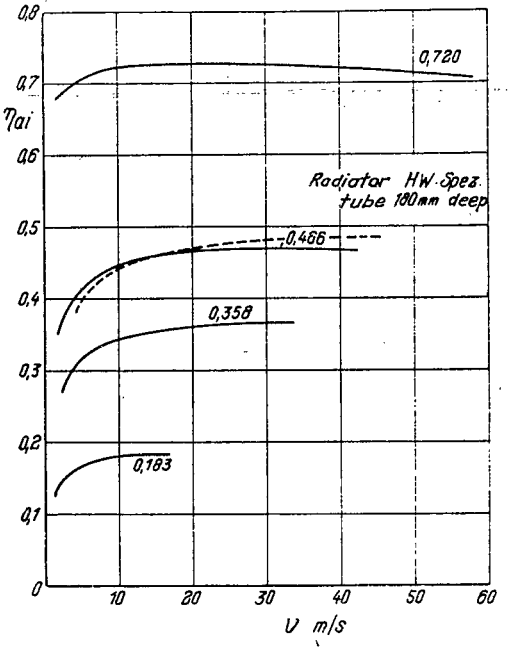

Figure 2.- Conductivity of screens and of radiator type H.W. Spez tube 180 plotted against rate of flow.

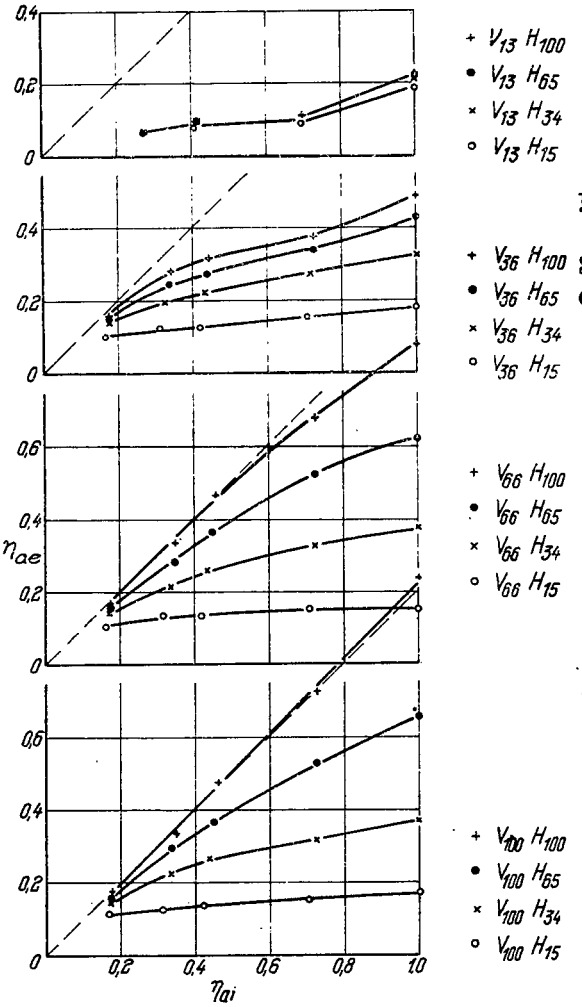

Figure 3.- Rate of flow coefficient against η_{ai}

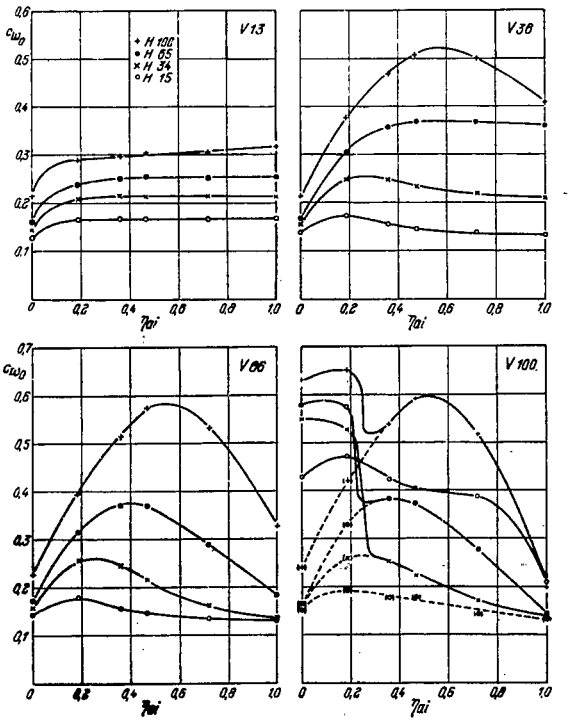

Figure 4.-Drag coefficients against η_{ai}

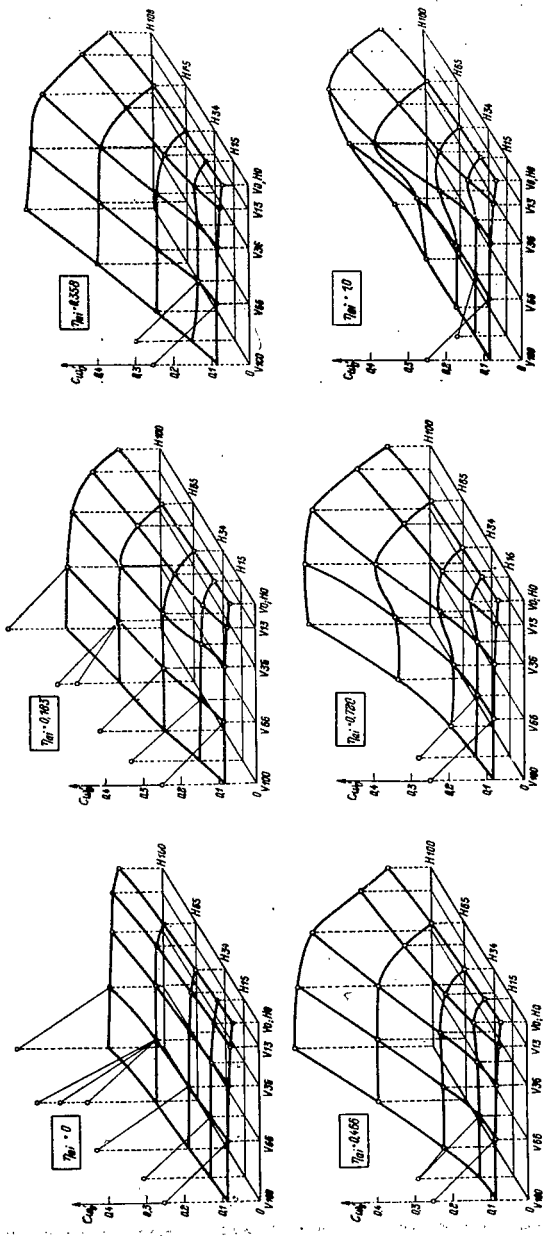

Figure 6.- Drag coefficients against opening ratios.

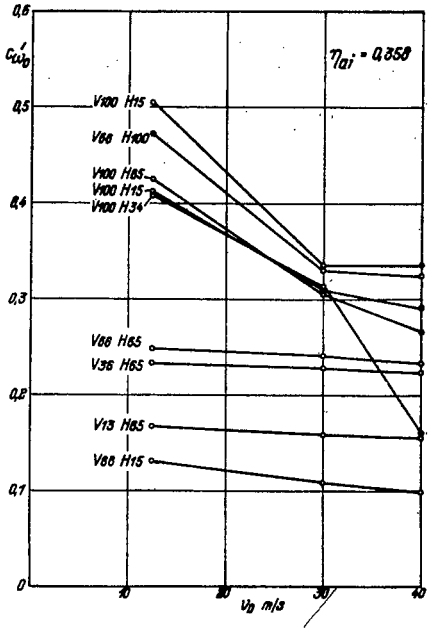

Figure 5.- Drag coefficients of several ducts plotted against v_o.

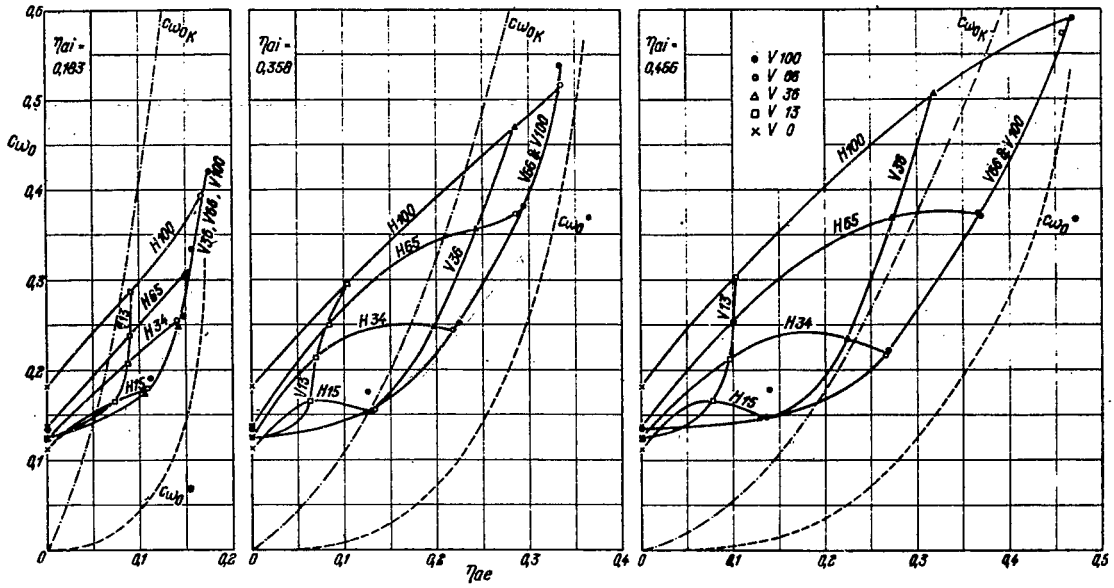

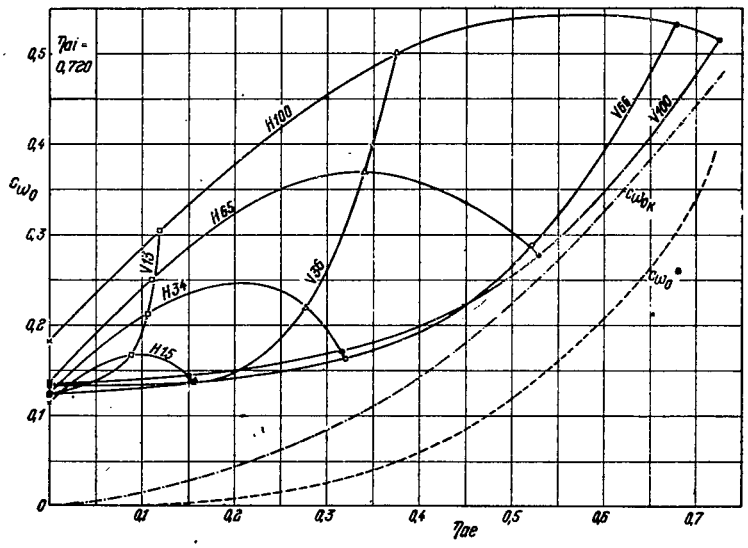

Figure 7.- Drag coefficients against η_{ae}

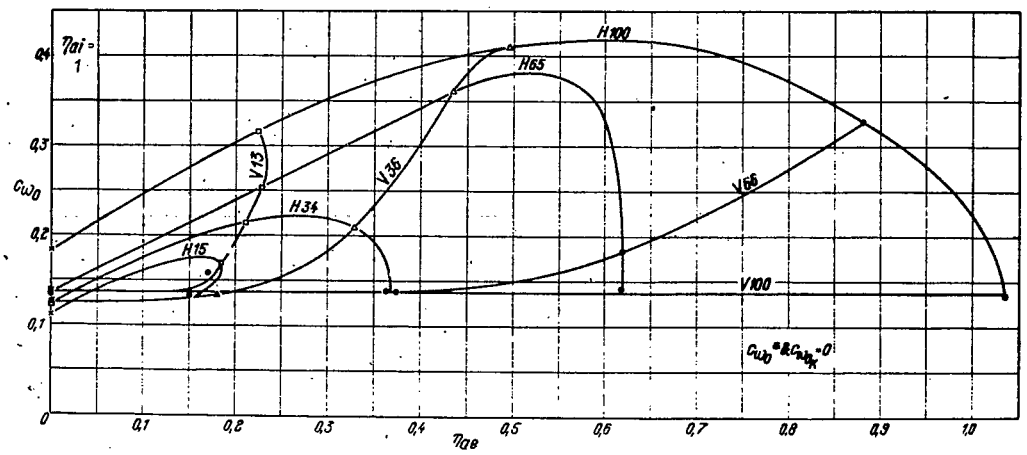

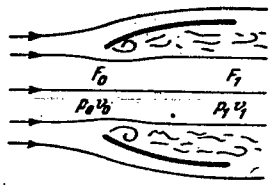

Figure 8.- Breakdown of flow on diffuser in free flow.

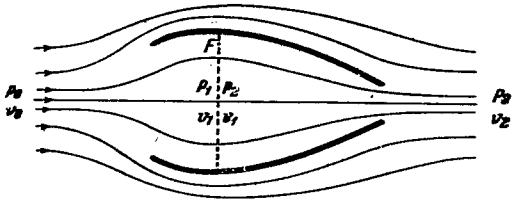

Figure 9.-Loss free flow on ducted radiator.

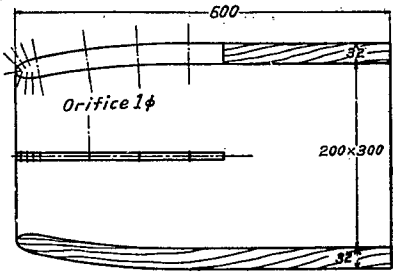

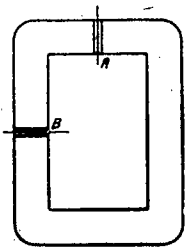

Figure 11.- Pressure orifice at sections A and B of diffuser V_{66}.

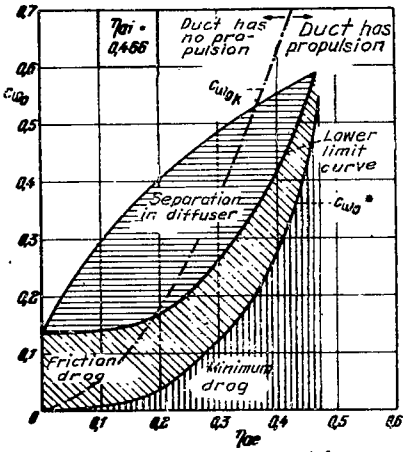

Figure 10.- Proportions of drag on ducted radiators. (η_{ai} = 0.466)

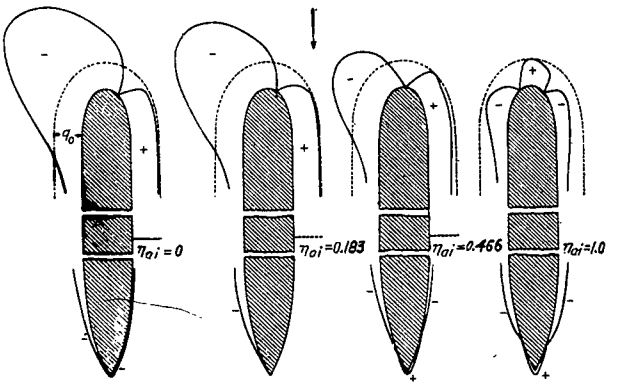

Figure 12.- Pressure distribution on V_{100} H_{100}.

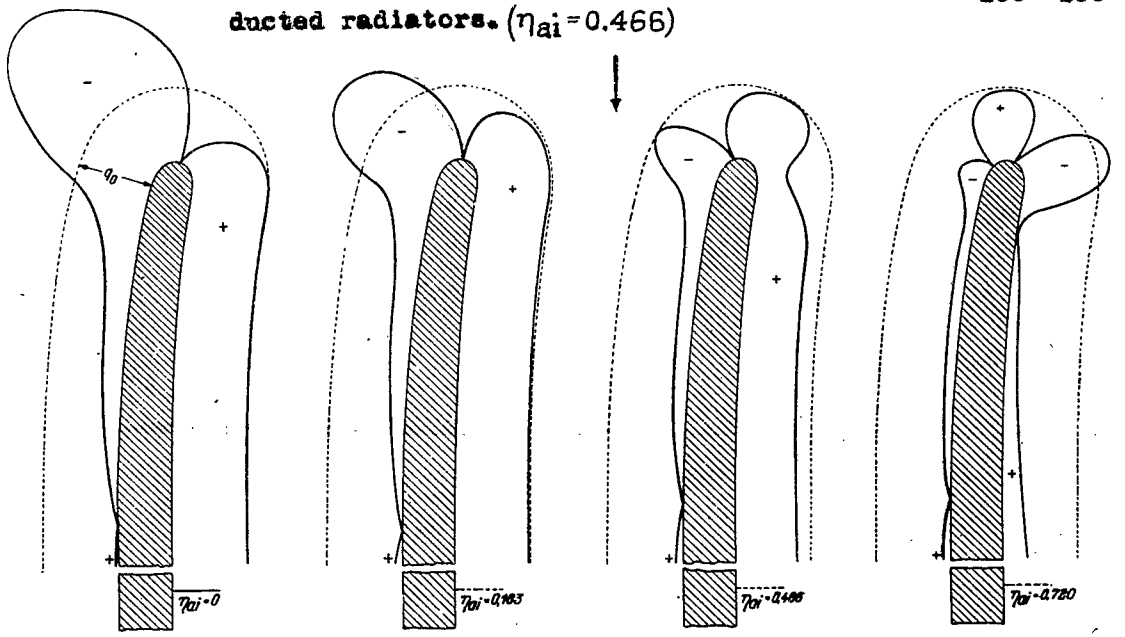

Figure 13.- Pressure distribution on V_{66}.

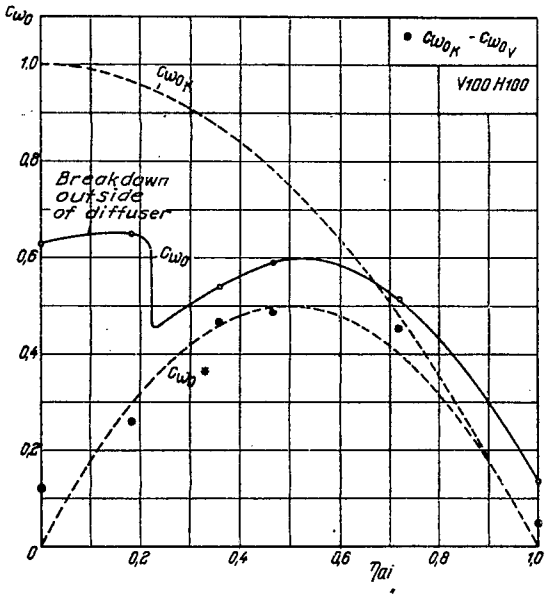

Figure 15.- $c_{woK} - c_{woV}$, c_{wo}, and c_{wo} with $V_{66}H_{100}$

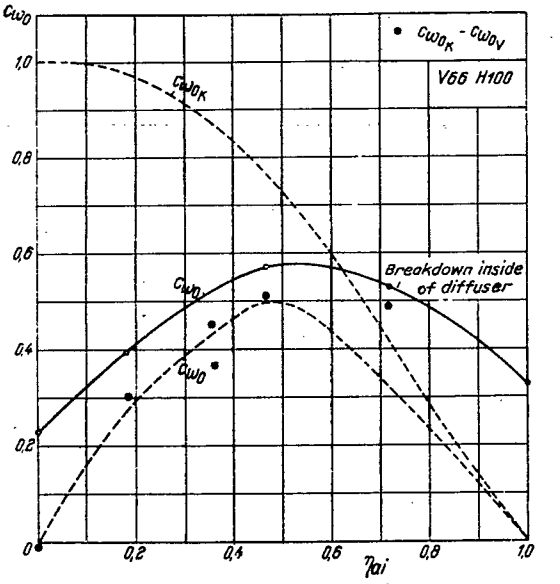

Figure14.- $c_{woK} - c_{woV}$, c_{wo}, and c_{wo} with $V_{100}H_{100}$.

Figure 16.- Thin walled ducted radiator with different exit opening ratios and different exit lengths.

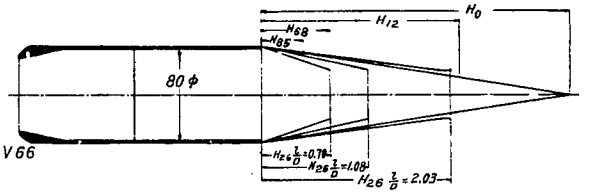

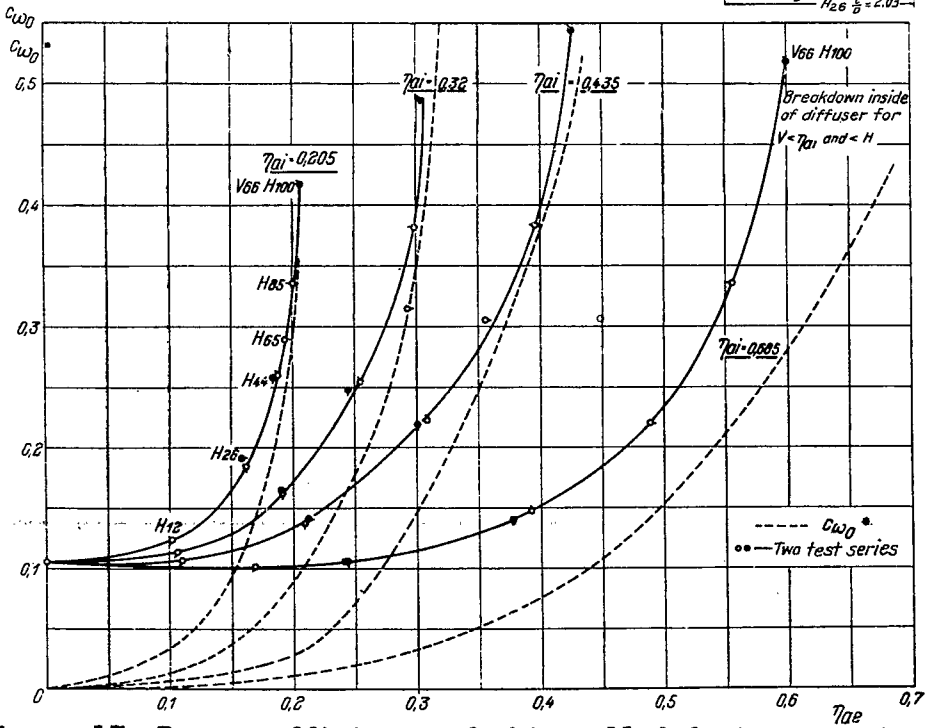

Figure 17.-Drag coefficients of thin walled ducts against η_{ae}.

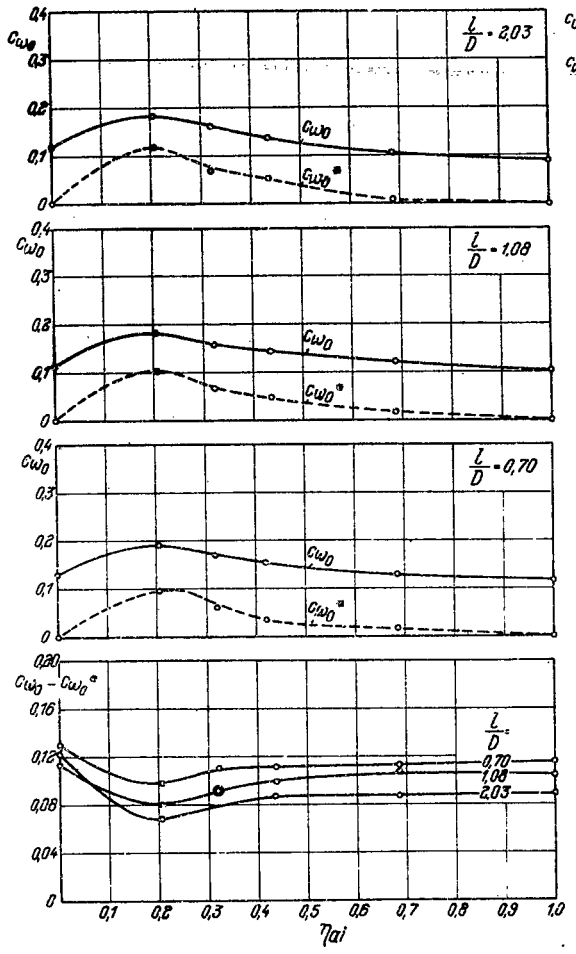

Figure 18.- Drag coefficient for $V_{66}H\ d_{26}$ at different l/D

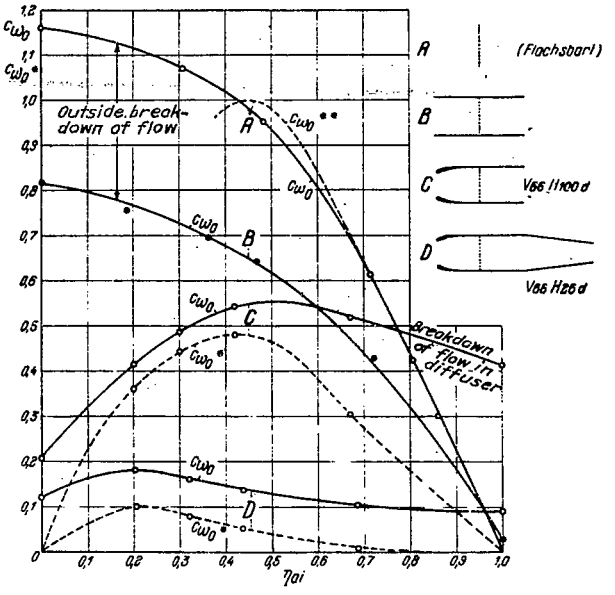

Figure 19.- Drag coefficient of typical duct designs against η_{ai}.

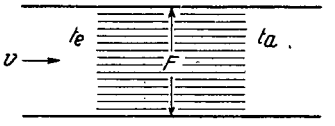

Figure 20.- Radiator block in tube (t_e and t_a = air temperature.)

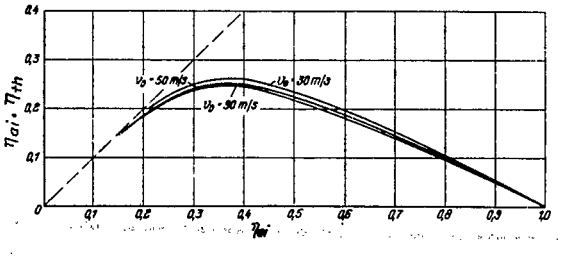

Figure 22.- Curves of maximum cooling power coefficient for cooler of 300mm depth, at different v_o.

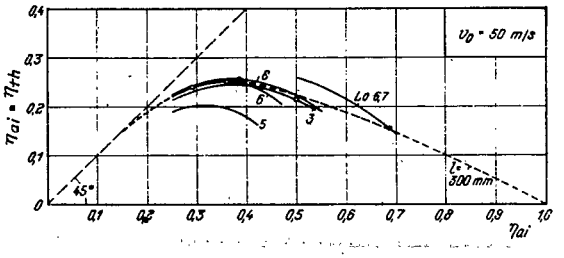

Figure 21.- Cooling power coefficients of different cooling systems against η_{ai} at v_o 50 m/s.

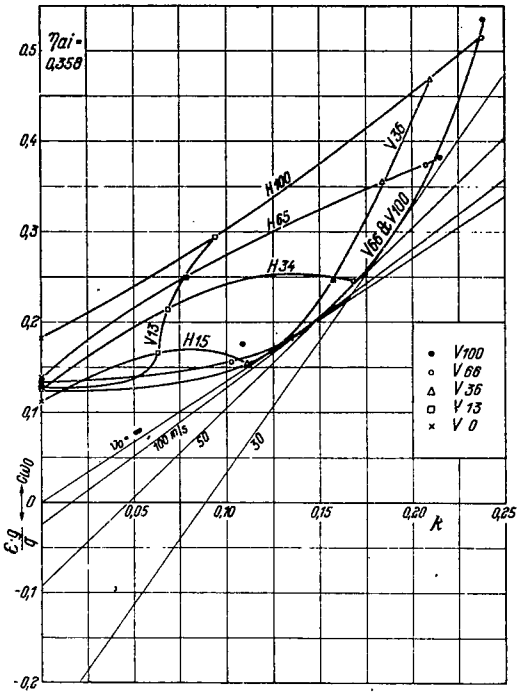

Figure 23.- Dragging power coefficient λ against cooling power coefficient at η_{ai} 0.358 .

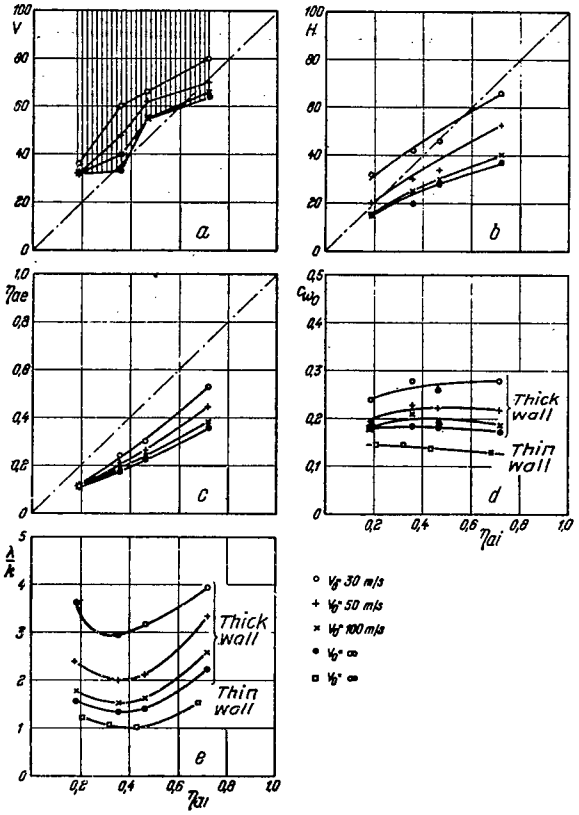

Figure 24(a to e).- Ratios of open areas, (a and b), flow coefficient, (c), drag coefficient, (d), and λ/κ (e), for ducted radiator with best λ.

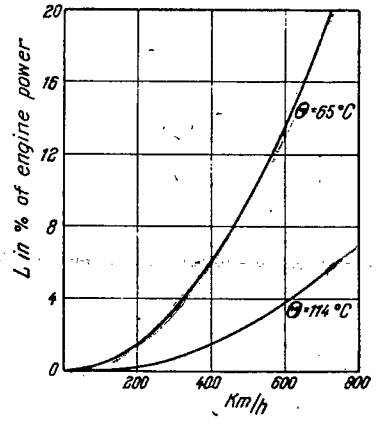

Figure 25.- Dragging power of best freely exposed ducted radiators plotted against flying speed— weight disregarded.